Small-Angle X-ray Scattering of DNA Fragments: Form and Interference Factors

Valeria Castelletto, Rosangela Itri, and Lia Q. Amaral*

Instituto de Física, Universidade de São Paulo, Caixa Postal 66318, CEP 05389-970, São Paulo, SP, Brazil

Gian P. Spada

Dipartamento di Chimica Organica "A. Mangini", Universitá di Bologna, via S. Donato 15, I-40127 Bologna, Italy

Received July 26, 1995®

ABSTRACT: Salt-free aqueous solutions of fragmented DNA are studied in the isotropic (I) phase in the semidilute regime until the I-cholesteric phase transition by a small-angle X-ray scattering technique (SAXS). The interference peak position q_m as a function of concentration fits an universal curve with exponent $^1/_2$ for an effective rod length $L = 340$ Å. The form factor of the DNA fragments is obtained from the less concentrated solution, where interference effects are not present in the measured range, and it is in good agreement with the B form of DNA. The interference curves for the more concentrated solutions are experimentally derived by dividing the corrected SAXS curve by the particle form factor. Modeling of the interference peaks with Gaussian functions compares well with recent theories for interparticle interactions on solution of rodlike polyelectrolytes. The peak broadening β expressed as βL in function of concentration also fits universal curve with exponent $^1/_2$. The fitting shows that the short-range order for rods in the semidilute region has a correlation length slightly above first neighbors.

Introduction

DNA molecules in solution show typical features common to several synthetic and biological polyelectrolytes and polymers in the form of long rods. With increasing concentration, the solution passes from a dilute regime to a semidilute regime and to liquid crystalline phases.[1-5] It has been recently found that aqueous solutions containing isolated plasmid DNA, at physiological DNA concentrations, form clusters characterized by a long-range lateral order.[6] Because DNA plays an essential role among the constituents of living systems, both an understanding of its phase behavior and a knowledge of its structural features at each phase are of fundamental importance.

Isotropic solutions of DNA are characterized by a maximum of intensity at low angles in the scattering curves caused by effects due to electrostatic interactions between the rods. It has been observed[7] that the angular position of this maximum, as for many other charged rodlike polyelectrolytes,[8-10] scales with the concentration C of particles as $C^{-1/3}$ for $C < C^*$ (dilute regime) and as $C^{-1/2}$ for $C > C^*$ (semidilute regime), where C^* is a critical concentration $C^* = 1$ particle/L^3, L being the rod length.

The $C^{-1/2}$ behavior, typical of the semidilute regime, has been explained in terms of scaling predictions.[11]

Small-angle X-ray scattering curves of DNA solutions in the semidilute regime have been investigated[7] focusing the influence of salt addition, which destroys the interference peak by screening the Coulomb potential between charged particles. But no detailed analysis of the experimental interference function has been so far reported.

Dilute isotropic solutions, in the presence or absence of the salt, have been studied by small-angle X-ray scattering (SAXS)[12] and small-angle neutron scattering (SANS)[13] techniques in order to investigate the counterion distribution around DNA, neglecting interparticle interference effects.

The interference factor $S(q)$ between charged rods has been experimentally derived for several polyelectrolytes,[8,9] but it is very difficult to calculate from known liquid theories. Unfortunately, up to now, there is no analytical solution such as that already developed for charged spherical colloids in a mean spherical approximation by solving the Ornstein–Zernicke equation.[14]

Initial attempts[15,16] to obtain an approximate $S(q)$ function for charged rods failed to reproduce the correlation maximum observed in experiments. Subsequent work by Klein and co-workers[17,18] using Monte Carlo simulations and perturbation theory was able to produce peaked $S(q)$ functions. A DLVO-Yukawa segment model was used to describe the interaction. Results by perturbation theory coincide with Monte Carlo simulations only for concentrations $C \leq C^*$ (diluted regime).[18]

Recent calculations using an *ab initio* approach, which combines molecular dynamics for the rods and the classical density functional theory for the counterions,[19] showed that the Yukawa segment model of Klein et al. is justified if the effective charges and the screening parameters are suitably chosen.

In the present study, we have investigated salt-free solutions of fragmented DNA by SAXS in several concentrations at room temperature in the isotropic (I) phase in the semidilute regime until the I–cholesteric (Ch) phase transition. No salt was added to the solutions in order to reach the most simple physical situation of the system. This also makes easier the comparison with theoretical results[17-19] obtained for salt-free solutions, where Coulombic interactions are not screened. Form and interference factors have been obtained as a function of concentration and compared with recent theories.[17-19]

® Abstract published in *Advance ACS Abstracts,* October 15, 1995.

0024-9297/95/2228-8395$09.00/0

Experimental Section

Salt-free samples with concentrations ranging from 10 to 202 mg/mL were prepared by mixing controlled amounts of fragmented DNA and deionized distilled water. Fragmented DNA was prepared by starting from highly polymerized calf thymus DNA (Sigma) which was sonicated with an Artek Ultrasonic 2000 (300 W) in short cycles for a total time of 1 h at a temperature between 0 and 5 °C. This technique produces considerable dispersion of fragment size. The molecular weight distribution was found to be around a maximum of 120 base pairs (bp) by agarose gel electrophoresis (the molecular weight marker was pBR322.*Hae*II with fragment lengths ranging from 8 to 587 bp). This corresponds to an average length of 400 Å and to a molecular weight of 85 000, but the broadening of the length distribution is about 20%. The DNA was recovered by ethanol precipitation. The mixture was kept at 5 °C for 24 h until equilibrium was reached. The concentration for each sample was calculated as C = mg of DNA/mL of solution.

Samples were conditioned in sealed 1-mm-diameter glass capillaries and investigated by SAXS at room temperature 22 ± 1 °C, since the temperature dependence of the phase transition is modest.[1-3] The Laue photographic method (punctual beam transmission geometry, Cu Kα Ni filter) with sample-to-film distance of about 10 cm was used. Scattering curves were obtained with a conventional small-angle Rigaku-Denki goniometer (line beam transmission geometry, Cu Kα graphite monocromator). The scattering intensity, J_{obs}, was corrected by subtracting the parasitic scattering (measured intensity without sample multiplied by the sample attenuation) and the electronic noise. The experimental points for scattering angles $2\theta < 0.4°$ (q = scattering vector = $2\pi s = (4\pi \sin(\theta))/\lambda < 0.029$ Å^{-1}) have been abandoned because of the strong influence of the direct beam.

Analysis Method. Linear 120-bp DNA fragments are considered as rigid rodlike cylinders.[20]

The SAXS intensity $I(q)$ of a fragmented DNA isotropic solution, corresponding to a system of interacting cylindrical particles, can be written as

$$I(q) = NF(q)S(q) \tag{1}$$

where N is the normalization factor, which includes the number density of particles as well as instrumental effects, $F(q)$ is the form factor of the particle, and $S(q)$ is the interparticle interference factor, which tends to unity for diluted noninteractive systems. It shall be noted that, in contrast to the case of spheres, $S(q)$ for long rods depends on the shape of the particles.[16,17]

In the case of rigid rodlike cylinders of length L and cross-sectional area A, when the radius of the transversal cross section R is such that $L \gg 2R$, $F(q)$ can be expressed as the product of two factors nearly independent leading to[21]

$$F(q) = L(\pi/q)I_c(q) \tag{2}$$

The form factor for the light scattering is that of a thin rod, being thus independent of the rod radius.[16,17] However, for X-rays, the R value defines the behavior of $I_c(q)$, the cross-sectional function given by

$$I_c(q) = \left(\frac{2\Delta\rho A J_1(qR)}{qR}\right)^2 \tag{3}$$

where J_1 is the first-order Bessel function and $\Delta\rho$ is the electron density contrast between the particle and the solvent.

For very small angles, $I_c(q)$ obeys the Guinier law:[21-22]

$$\lim_{q\to 0} I_c(q) = A^2(\Delta\rho)^2 e^{-(q^2R_c^2/2)} \tag{4}$$

where R_c is the radius of gyration of the cylinder cross section ($R_c = R/2^{1/2}$) and its value can be evaluated from the plot of $\log(I_c(q))$ vs $\log(q^2)$ (Guinier plot).

Furthermore, the cross-sectional distance distribution function, $p_c(r)$, is also of great help in the data analysis being related to $I_c(q)$ through[23]

$$p_c(r) = \frac{1}{2\pi}\int_0^\infty I_c(q) q r J_0(qr)\, dq \tag{5}$$

where J_0 is the zero-order Bessel function. R_c can be also calculated from $p_c(r)$ using the whole available scattering curve:

$$R_c^2 = \frac{\int_0^\infty r^2 p_c(r)\, dr}{2\int_0^\infty p_c(r)\, dr} \tag{6}$$

providing more accurate results than the Guinier approximation.

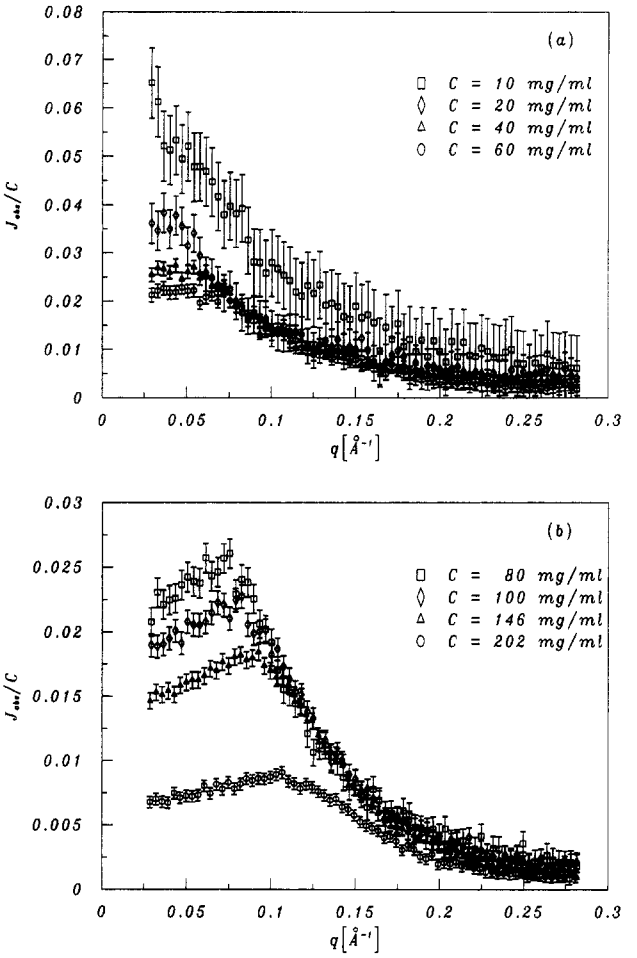

Figure 1. Small-angle X-ray scattering curves divided by C: (a) 10, 20, 40, and 60 mg/mL (10 mg/mL curve has been plotted only up to q = 0.282 Å^{-1}); (b) 80, 100, 146, and 202 mg/mL.

The indirect transformation process (ITP) developed by Glatter[24] was used in our work to calculate $p_c(r)$ for the lowest concentration as well as to get the desmeared scattering curve J_{desm} corrected from the X-ray line geometry effects since, as will be shown in the next section, the interference effect is not pronounced over the measured scattering curve for such concentration. Details of the procedure are similar to those for spherical particles and can be found in ref 25.

The indirect transformation process in reciprocal space (ITR), recently developed by Glatter,[26] was used for higher concentrations since it allows calculation of J_{desm} for partially ordered systems, i.e., systems that present peaks in J_{obs}. The algorithm of this method has already been described in the literature:[24,26] J_{desm} is approximated by a sum of N cubic B-spline functions, and a stable solution for J_{desm} is reached selecting the Lagrangian multiplier λ_{opt} by the point of inflection method.[24,25]

$S(q)$ curves can be experimentally derived dividing J_{desm} in eq 1 by the modeled $F(q)$.

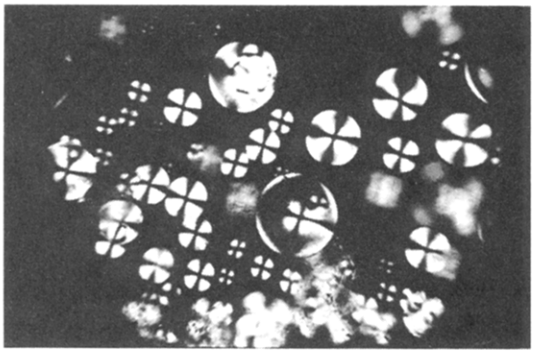

Figure 2. Small spherulites in coexistence with the isotropic phase obtained by evaporation of a sample with 202 mg/mL, observed by polarized microscopy.

Results

Figure 1 presents SAXS curves in the studied interval of 10−202 mg/mL divided by the concentration C. The decrease of intensity with concentration is due to the increasing interparticle interference effects. The range of concentration studied in our work is in the semidilute regime.

The scattering curve for 10 mg/mL does not show any structure; an interference peak begins to appear in the scattering curve for higher concentrations, moving to larger angles with increasing concentration.

Neither observations by polarized microscopy nor the SAXS curves have shown in our samples the formation of liquid crystalline domains within the solution. Strzelecka and Rill[2] found the first indication of weakly "birefringent" phase domain formation in coexistence with the I phase at 133 mg/mL for low-salt solutions of 500-Å DNA. The length of our fragments is smaller, and this probably increases their freedom of rotation at a given concentration, raising the concentration of anisotropic phase formation. This was confirmed by observation of small spherulites in coexistence with the I phase by evaporation of a sample with 202 mg/mL (Figure 2).

Particle Form Factor. Interparticle interactions are present in the whole concentration range studied, and it is not possible in general to obtain $I_c(q)$ from $I(q)$ since $S(q) \neq 1$. However, the interference peak for the smallest concentration falls below the measured q region, and the approximation $S(q) = 1$ can be tested in the measured q range.

Therefore both ITP and ITR programs have been used to analyze the data for 10 mg/mL. Several tests showed that ITR was unable to reconstruct any interference peak distinguishable from noise ripples, while ITP provided the best possible results.

It was considered meaningful therefore to obtain information about the shape of the DNA fragments, calculating $p_c(r)$ from J_{obs} for 10 mg/mL by using the ITP program.[23,24] It was necessary to measure points up to $q = 0.654$ Å^{-1} on the SAXS curve to reach a good resolution in our results. The number of spline functions used was 15. According to the rules established by the point of inflection method,[24,25,27] λ_{opt} was found to correspond to 7.

Figure 3 presents the $p_c(r)$ function obtained for 10 mg/mL. An extra background was extracted, and points for q <0.039 Å^{-1} have been neglected to avoid scattering background and concentration effects in $p_c(r)$.[28] Due to the high value of the errors, $p_c(r)$ slightly deviates from zero at $r = 0$ Å but it drops to zero at $r = D_{max} = 21.68 \pm 0.06$ Å, giving $R = 10.84 \pm 0.03$ Å and a value for R_c of 7.91 ± 0.02 Å, in good agreement with the B form of

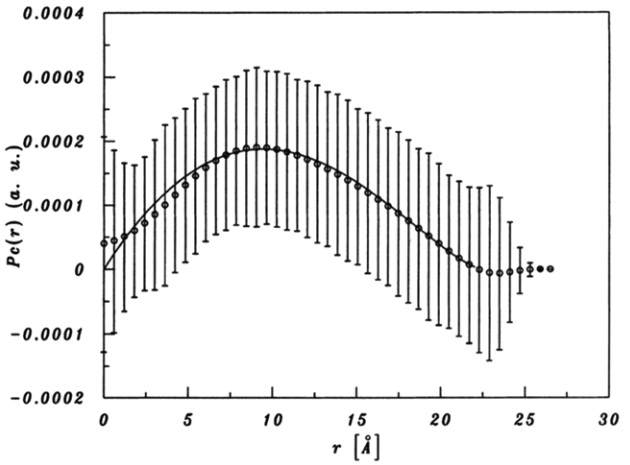

Figure 3. Cross-sectional distribution function for 10 mg/mL. (○) $p_c(r)$ calculated by using the ITP program; (—) exact $p_c(r)$ of a homogeneous circular cylinder: $p_c(r)$ = constant[arccos-$(r/2R) - (r/2R)(1 - (r/2R)^2)$] evaluated for $2R = 21.68$ Å.

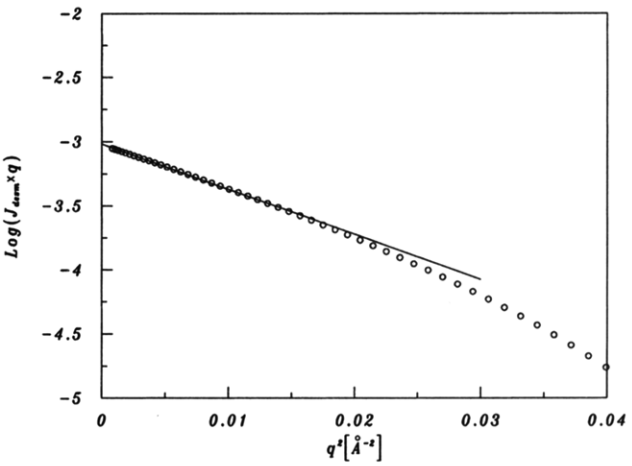

Figure 4. Guinier plot for 10 mg/mL.

DNA.[12,29] The exact $p_c(r)$ of a homogenous circular cylinder as given by Porod[30] is shown in Figure 3, showing a good agreement between both curves. No evidence of inhomogeneities of the density charge distribution on the cross section of the cylinders is observed in the form of $p_c(r)$. Figure 4 shows the Guinier plot of the corresponding desmeared scattering curve, providing a R_c value of 8.4 ± 0.4 Å, also in agreement with previous measurements by this method.[29,31] This value is more inexact and differs by 6% from that of the $p_c(r)$ analysis, but the difference is within the experimental error.

The SAXS curve for 10 mg/mL was also fitted by modeling the double helix of DNA in an infinite cylindrical shape, according to eqs 2 and 3 convoluted with the slit length smearing effect. The best fitting was obtained with $R = 10.84$ Å (Figure 5), the same value obtained from the $p_c(r)$ function.

The results from the modeling of the scattering curve for 10 mg/mL demonstrates that DNA fragments behave as "infinite cylinders" in solution, in agreement with several tests showing that the infinite cylinder condition is lost only in the range $L/2R \leq 12$.

The procedure of using the data for the smallest concentration to obtain the particle form factor led to consistent results. The basic factor allowing this approach is the nonappearance of interference effects in the measured q range, together with careful desmearing techniques.

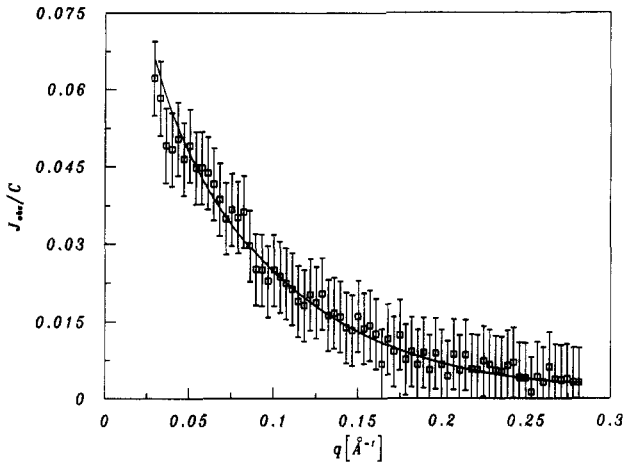

Figure 5. Small-angle X-ray scattering curve for 10 mg/mL: (—) $F(q)$ according to eqs 2 and 3 convoluted with the smearing effect of the slit length (10 mg/mL curve has been plotted only up to $q = 0.282$ Å^{-1}).

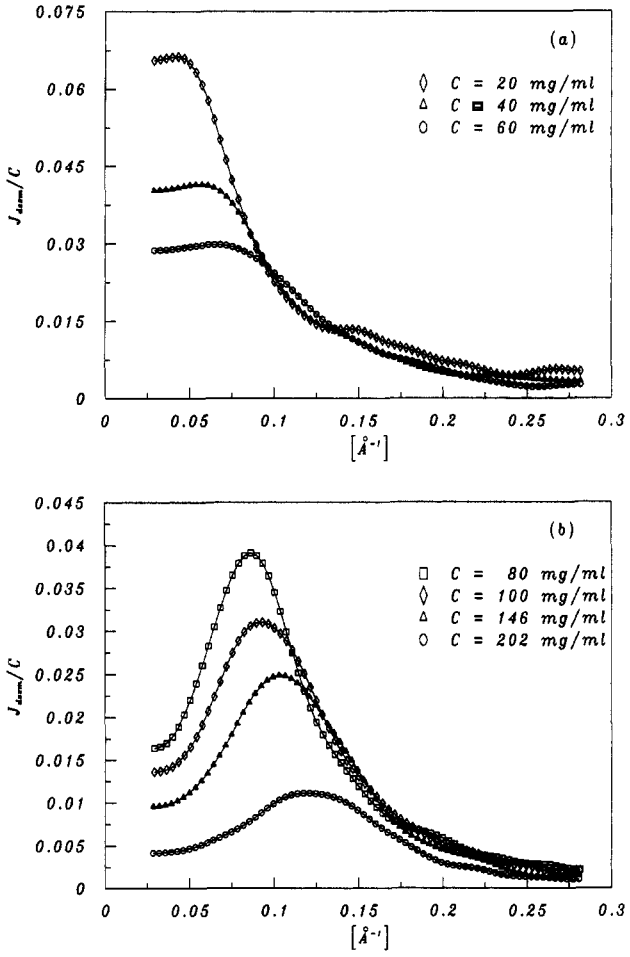

Figure 6. Small-angle X-ray scattering curves desmeared from slit length and slit width effects by using the ITR program: (a) 20, 40, and 60 mg/mL; (b) 80, 100, 146, and 202 mg/mL.

Interference Function. The ITR process[26,27] was used to deconvolute the SAXS curves from the X-ray slit length and slit width effects for $C \geq 20$ mg/mL, in which the interference effects start to appear on the measured curves. Figure 6 shows the resulting desmeared curves. The interference peak position s_0^{-1} ($q_m = 2\pi s_0$) was measured from all the desmeared SAXS curves and for the higher concentrations from the Laue technique, which was unable to detect the very weak scattering for the lower concentrations. The s_0^{-1} values

Table 1. Values of Interference Peak Position and Parameter Values Obtained by Modeling the First Peak in the Experimental Structure Factor Curves by Using a Gaussian Function[a]

C (mg/mL)	$[s_0^{-1}]_L$ (Å)	$[s_0^{-1}]_{dec}$ (Å)	$\overline{s_0^{-1}}$ (Å)	$[s_0^{-1}]_g$ (Å)	β (Å^{-1})
20		145 ± 10		110	0.052
40		109 ± 6		82	0.064
60		92 ± 4		69	0.089
80	76 ± 2	73 ± 3	75 ± 3	63	0.068
100	67 ± 2	70 ± 2	68 ± 2	55	0.085
146	57 ± 1	61 ± 2	59 ± 2	48	0.092
202	50 ± 2	52 ± 1	51 ± 2	41	0.101

[a] The values include the following: concentration of the sample C, scattering peak position measured by the Laue method $[s_0^{-1}]_L$, scattering peak position of the peak deconvoluted from slit length and slit width effects $[s_0^{-1}]_{dec}$, average value $\overline{s_0^{-1}}$, Gaussian peak position $[s_0^{-1}]_g$, and Gaussian width at middle height β.

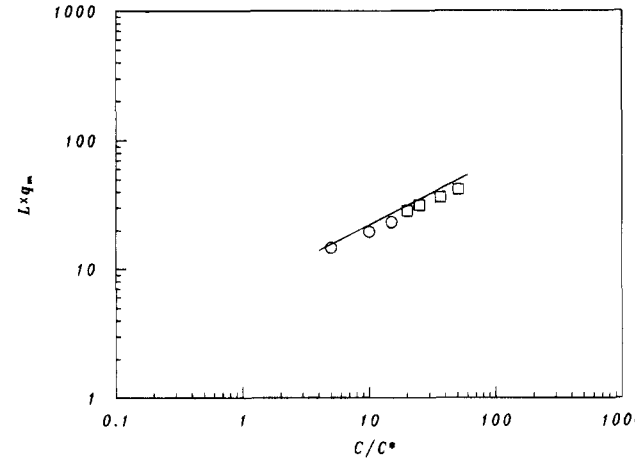

Figure 7. Scattering peak position, s_0^{-1}, as a function of the concentration C: (○) $[s_0^{-1}]_{dec}$ values; (□) averages values between $[s_0^{-1}]_L$ and $[s_0^{-1}]_{dec}$; (—) universal curve that fitted previous data of DNA and other rod systems.[7]

are listed in Table 1 and are fitted to

$$s_0^{-1} = (587 \pm 72)C^{-(0.46\pm0.03)} \quad (7)$$

As expected, the relation $s_0^{-1} \propto C^{-1/2}$ is valid in eq 7 within the experimental error.

Results with the same exponent have been experimentally observed for solutions of 500-Å DNA fragments at low salt in the semidilute regime using SAXS[7] and at the I−Ch transition and Ch phase using SANS,[5] demonstrating that this behavior persists through the phase transition and also within the Ch phase. A single broad peak with $s_0^{-1} \propto C^{-1/2}$ behavior was also observed at low angles in the scattering curves of salt-free solutions of several polyelectrolytes[8-10] in the semidilute regime.

Figure 7 shows the universal curve q_mL as function of C/C^*, which fitted previous data on DNA and other rod systems.[7-10]

$$q_mL = 7.00(C/C^*)^{0.5} \quad (8)$$

A reasonable agreement between our data and the universal curve is obtained using $L = 340$ Å (100 bp) as an effective value for the dispersed distribution of rod lengths. This value is used to obtain our q_mL values, presented in Figure 7. With this L value, the critical concentration of our sample is[9] $C^* = 2.544 \times 10^{17}$ fragments of DNA/mL ~ 4 mg/mL, and our concentration range is $2.5C^* \geq C \geq 50.5C^*$.

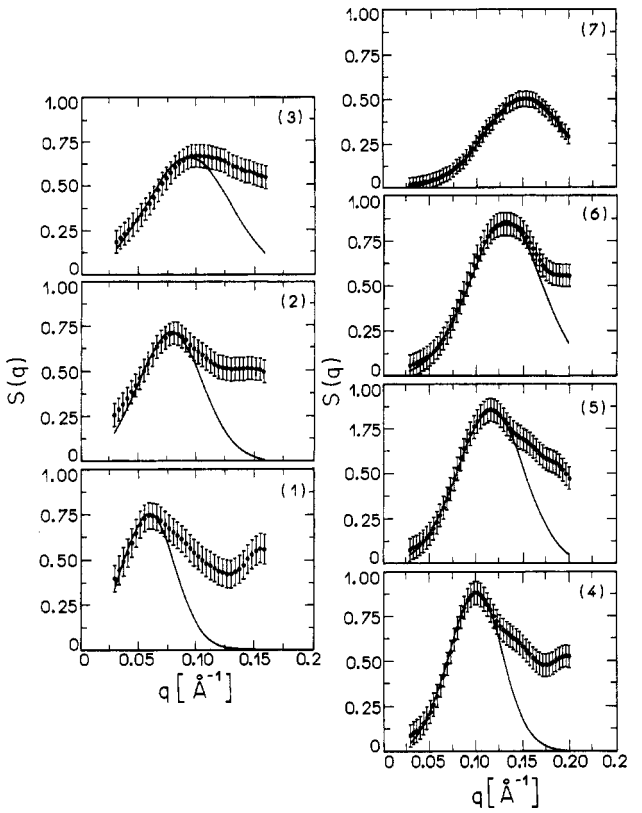

Figure 8. (O) Experimental structure factor; (—) modeling obtained with a Gaussian function (parameters for modeling are listed in Table 1): (1) 20, (2) 40, (3) 60, (4) 80, (5) 100, (6) 146, and (7) 202 mg/mL.

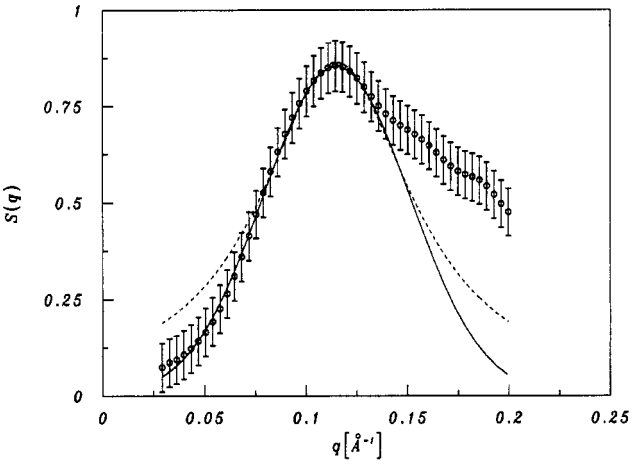

Figure 9. (O) Experimental structure factor for 100 mg/mL ($C/C^* = 25$): (—) modeling with a Gaussian function (parameters for modeling are listed in Table 1); (···) modeling with a Lorentzian function.

In the interval of concentrations 20–202 mg/mL, $S(q)$ was experimentally derived dividing J_{desm}, normalized in relation to C, by the form factor modeled for 10 mg/mL. Points with $q > 0.157$ Å^{-1} for 20–60 mg/mL and with $q > 0.199$ Å^{-1} for 80–202 mg/mL were not used to calculate $S(q)$ due to the fluctuations in J_{desm}. Figure 8 shows the experimental structure factor curves derived.

Gaussian and Lorentzian functions were tested to model the peaks of $S(q)$. For higher concentrations, a better modeling of the inner part of the curves was reached using Gaussian functions, as shown in Figure 9 for the 100 mg/mL $S(q)$ curve. This could not be observed for 20–60 mg/mL because points with $q <$ 0.029 Å^{-1} were abandoned due to the strong influence of the direct beam, and the information at very low angles where this effect is present were lost.

The modeling of the first peak of the experimental structure factors with Gaussian functions is plotted together with the corresponding $S(q)$ curves in Figure 8. Table 1 also lists the values of the parameters obtained from these modelings: β and $[s_0^{-1}]_g$ are the width at middle height (measured in q units) and the peak position of the Gaussian curve. It is important to remark that, although β values progressively increase with C, the value for 60 mg/mL is out of this sequence. The ITR process produces a curve plane in the inner part, probably due to systematic errors in the desmearing process,[26] and with approximately the same inclination of the particle form factor curve for 0.1 Å$^{-1} \leq q \leq$ 0.157 Å^{-1}, leading to an excessively broad and less well defined interference peak in this particular curve.

Values $[s_0^{-1}]_g$ also show a dependence with concentration with an exponent of $^1/_2$, within the experimental errors.

Discussion

We shall now compare our $S(q)$ curves with available data obtained both experimentally and theoretically in semidilute solutions of rods.

The main peak in the $S(q)$ curves becomes broader with increasing concentration, as can be inferred from the parameters of the Gaussian function fitting these curves, listed in Table 1. Broadening increasing with C was also obtained experimentally by static light scattering in semidilute solutions of rodlike fd virus (L = 8800 Å, $2R$ = 60 Å).[9]

Concerning theoretical work, Canessa and co-workers[18] calculated Monte Carlo simulations for solutions of charged polyelectrolytes (modeled according to the rodlike tobacco mosaic virus) with $0.05\ C^* \geq C \geq 4C^*$, considering interparticle interactions between segments situated on each fragment via a Yukawa potential.

An analysis of the results for $S(q)$ obtained by Canessa et al. showed that the peak position goes with $C^{-1/3}$ in the dilute region. In the semidilute region, the Monte Carlo results show a deviation that fits a $C^{-1/2}$ behavior, while the results by perturbation remain with a $C^{-1/3}$ behavior.

The Monte Carlo results[18] show that the deviation from $C^{-1/3}$ behavior is due to the dependence of the interaction on the rod length; the effect of angular correlations makes it necessary to take into account higher spherical harmonic coefficients of the pair correlation function, which start to contribute significantly for $C \geq C^*$ and are not present in the perturbation approximation.

Data on Figure 10 have been extracted from ref 18 and correspond to the resulting Monte Carlo structure factor plotted vs qL for the semidilute regime ($C = 4C^*$). There is a strong similarity between our results for C/C^* = 25 (Figure 9) and Monte Carlo results for $C/C^* = 4$ (Figure 10): a single not completely well defined peak is observed in the $S(q)$ curve, and the modeling of the inner part of the curve provided by a Gaussian function is better than that obtained by using a Lorentzian function. We have also arrived at the same results testing Gaussian and Lorentzian functions to model the peak on experimental $S(q)$ curves for the fd virus in the semidilute region, extracted from ref 9.

For all these cases, the Gaussian shape of the structure factor ensures that the correlation function does not have a simple exponential decay with increasing average distance between the rods, in agreement

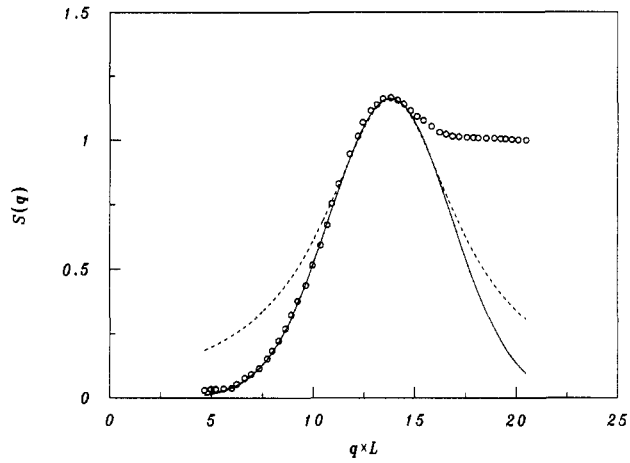

Figure 10. (◇) Theoretical structure factor from Monte Carlo simulation for a semidilute solution ($C/C^* = 4$) of charged polyelectrolytes modeled according to the tobacco mosaic virus:[18] (—) modeling with a Gaussian function; (···) modeling with a Lorentzian function.

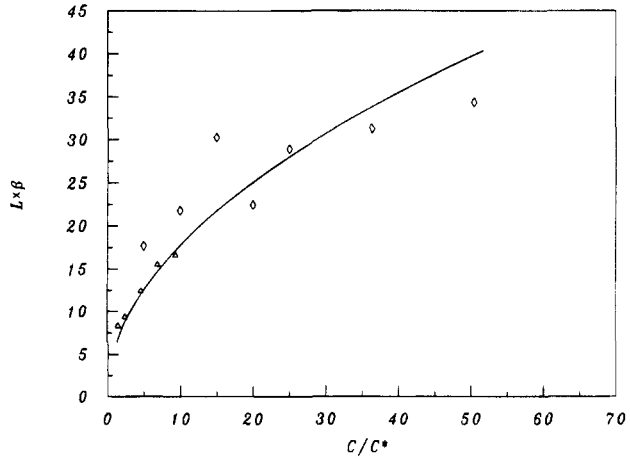

Figure 11. Plot of the width at middle height β of the Gaussian functions modeling the structure factor peaks, in terms of βL vs C/C^*: (◇) DNA; (△) fd virus.[9]

with the potential used for the interparticle interactions in the Monte Carlo simulation.[18]

In order to have a means of comparison of available data for $S(q)$ obtained for systems with different rod length and in different concentration regions, a more universal plot was searched.

Figure 11 shows the variation of βL vs C/C^* for our DNA results and for the fd virus[9] in the semidilute region, as well as a fitting with exponent $^1/_2$:

$$L\beta = (5.6 \pm 0.7)(C/C^*)^{0.5} \quad (9)$$

From eqs 7–9, a direct relation is obtained between β and q_m, independent of L and concentration, valid for the semidilute region:

$$\beta = (0.8 \pm 0.2)q_m \quad (10)$$

This leads to a correlation length

$$l = 2\pi/\beta = (1.25 \pm 0.2)s_0^{-1} \quad (11)$$

This result seems to be "universal" for the semidilute region and says that the correlation slightly exceeds first neighbors, but does not fully reach second neighbors.

It is also clear that the broadening of the interference peak with concentration is a direct result of the dependence of the peak position with $C^{-1/2}$ and not of a change in the degree of order with concentration.

Figure 11 also shows a slight tendency for deviation toward smaller broadening at very high concentration. This could indicate an increase in the degree of short-range order near the I–Ch phase transition, but the dispersion of β values at smaller concentrations is too large for a conclusion on this point.

Acknowledgment. The interest of Prof. G. Gottarelli was important to define this collaboration. Thanks are due to Dr. Otto Glatter for helpful discussions and to O. Santin Filho for the photograph of Figure 2. The financial support of FINEP, FAPESP, and CNPq foundations is acknowledged. V.C. has a Ph.D. fellowship from CNPq.

References and Notes

(1) Strzelecka, T. E.; Rill, R. L. *J. Am. Chem. Soc.* **1987**, *109*, 4513. Strzelecka, T. E.; Davidson, M. W.; Rill, R. L. *Nature* **1988**, *331*, 457. Strzelecka, T. E.; Rill, R. L. *Macromolecules* 1991, *24*, 5124.
(2) Strzelecka, T. E.; Rill, R. L. *Biopolymers* **1990**, *30*, 57.
(3) Spada, G. P.; Brigidi, P.; Gottarelli, G. *J. Chem. Soc., Chem. Commun.* **1988**, *14*, 953. Gottarelli, G.; Spada, G. P.; Mariani, P.; Miranda de Morais, M. *Chirality* **1991**, *3*, 227.
(4) Durand, D.; Doucet, J.; Livolant, F. *J. Phys. II Fr.* **1992**, *2*, 1765.
(5) Groot, L. C. A.; Kuil, M. E.; Leyte, J. C.; Van der Maarel, J. R. C.; Heenan, R. K.; King, S. M.; Jannik, G. *Liq. Cryst.* **1994**, *17*, 263.
(6) Reich, Z.; Watchel, E. J.; Minsky, A. *Science* **1994**, *264*, 1460.
(7) Wang, L.; Bloomfield, V. A. *Macromolecules* **1991**, *24*, 5791.
(8) Maier, E. E.; Schulz, S. F.; Weber, R. *Macromolecules* **1988**, *21*, 1544.
(9) Schultz, S. F.; Maier, E. E.; Weber, R. J. *J. Chem. Phys.* **1989**, *90*, 7.
(10) Drifford, M.; Dalbiez, J. P. *J. Phys. Chem.* **1984**, *88*, 5368.
(11) Koyama, R. *Macromolecules* **1984**, *17*, 1594; **1986**, *19*, 178. de Gennes, P. G.; Pincus, P.; Velasco, R. M.; Brohand, F. *J. Phys.* **1987**, *87*, 3008.
(12) Chang, S.; Chen, S.; Rill, R. L.; Lin, J. S. *J. Phys. Chem.* **1990**, *94*, 8025. Chang, S.; Chen, S.; Rill, R. L.; Lin, J. S. *Colloid Polym. Sci.* **1991**, *84*, 409.
(13) Van der Maarel, J. R. C.; Groot, L. C. A.; Mandel, M.; Jesse, W.; Jannik, G.; Rodriguez, V. *J. Phys. II Fr.* **1992**, 2, 109.
(14) Hayter, J. B.; Penfold, J. *Mol. Phys.* **1980**, *42*, 109. Hansen, J. P.; Hayter, J. B. *Mol. Phys.* **1982**, *46*, 651. Itri, R.; Amaral, L. Q. *Phys. Rev. E* **1993**, *47*, 2551.
(15) Benmouna, M.; Weill, G.; Benoit, H.; Akcasu, Z. *J. Phys. Fr.* **1982**, *43*, 1679.
(16) Schneider, J.; Hess, W.; Klein, R. *J. Phys. A* **1985**, *18*, 1221.
(17) Schneider, J.; Hess, W.; Klein, R. *Macromolecules* **1986**, *19*, 1729. Schneider, J.; Karrer, D.; Dhant, J. K. G.; Klein, R. *J. Chem. Phys.* **1987**, *87*, 3008.
(18) Canessa, E.; D'Aguanno, B.; Weyerich, B.; Klein, R. *Mol. Phys.* **1991**, *73*, 175.
(19) Löwen, H. *J. Chem. Phys.* **1994**, *100*, 6738.
(20) Nicoliei, T.; Mandel, M. *Macromolecules* **1989**, *22*, 2348.
(21) Glatter, O. *Small Angle X-ray Scattering*; Academic Press: London, 1982.
(22) Guinier, A.; Fournet, G. *Small Angle Scattering of X-rays*; Wiley: New York, 1955.
(23) Glatter, O. *J. Appl. Crystallogr.* **1980**, *13*, 577.
(24) Glatter, O. *J. Appl. Crystallogr.* **1979**, *12*, 166; **1977**, *10*, 415.
(25) Itri, R.; Amaral, L. Q. *J. Phys. Chem.* **1991**, *95*, 423. Itri, R.; Amaral, L. Q. *J. Appl. Crystallogr.* **1994**, *27*, 20.
(26) Glatter, O.; Gruber, K. *J. Appl. Crystallogr.* **1993**, *26*, 512.
(27) Article in preparation.
(28) Müller, K.; Glatter, O. *Makromol. Chem.* **1982**, *183*, 465.
(29) Bram, S.; Beeman, W. W. *J. Mol. Biol.* **1971**, *55*, 311.
(30) Porod, G. *Acta Phys. Austriaca* **1948**, *2*, 255.
(31) Luzzati, V.; Masson, F.; Mathis, A.; Saledjian, P. *Biopolymers* **1967**, *5*, 491.

MA9510855